Carbon nanofiber-PEDOT composite films as novel microelectrode for neural interfaces and biosensing

Valentin Saunier [a], Emmanuel Flahaut [b], Marie-Charline Blatché [a], Christian Bergaud [a,*], Ali Maziz [a,**]

[a] LAAS-CNRS, Université de Toulouse, CNRS, F-31031 Toulouse, France
[b] CIRIMAT, Université de Toulouse, CNRS, 118 route de Narbonne, F-31062, Toulouse, France

Keywords:
PEDOT:CNF
Microelectrodes
Neural interfaces
Electrical stimulation
Electrochemical sensing
Carbon nanofibers

A B S T R A C T

A clear need exists for novel nanostructured materials that are capable to meet the performance criteria of a number of neuronal therapies including neural recording, stimulation and sensing of bioactive molecules at the electrode-tissue interface. By combining Poly (3,4-ethylenedioxythiophene) (PEDOT), with Carbon Nanofibers (CNFs), we demonstrate a versatile approach for the synthesis of a novel composite material PEDOT:CNF with remarkable electrochemical properties, combining low impedance, high surface area, high charge injection capability and reliable neurotransmitters monitoring using amperometric techniques. The oxidized CNFs were utilized as dopants of PEDOT to prepare the composite coatings through electrochemical deposition on neural microelectrodes arrays (MEA). The PEDOT:CNF modified microelectrodes demonstrated the low specific impedance of 1.28 MΩ μm^2 at 1 kHz and results in unrivalled charge injection limit of 10.03 mC/cm^2 when compared to other reported organic electrode nanomaterials. Furthermore, amperometric detection performances were determined for the neurotransmitters dopamine and serotonin, exhibiting linear concentration range from 0.1 to 9 μM and from 0.06 to 9 μM respectively, high sensitivities (44.54 pA/nM.μm^2 and 71.08 pA/nM.μm^2, respectively) and low detection limits (0.045 μM and 0.056 μM, respectively). Cell viability was investigated on PEDOT:CNF coated microelectrodes to show that the composite material does not advocate any cytotoxicity. Taken together, these results suggest the great potential of PEDOT:CNF composite for developing next-generation multifunctional microelectrodes for applications in neural therapies.

1. Introduction

Technological approaches based on either electrical stimulation or neural recording involve the use of microelectrodes interfaced with a population of single neurons in close proximity (Ludwig et al., 2006; Nicolelis et al., 2003). Noble metals such as Platinum, or Iridium have been used for decades to make arrays of microscopic electrodes, which are now used in routine for neural recording and stimulation in several clinical contexts such as cochlear implants, deep brain stimulation for Parkinson's disease, or functional evaluation of epilepsy(Andrews, 2009; Rebscher et al., 2008; Wagenaar et al., 2005). However, the drawback of metallic electrodes is their limited capability of safe neural stimulation (Heim et al., 2012), high intrinsic noise level for neural recording (Cogan, 2008) and the mechanical mismatch between the electrode and surrounding tissue causing failure of the device (Polikov et al., 2005).

To overcome these limitations, research in nanostructured materials have received much attention for developing next-generation neural interfaces, which focused on improving charge storage capacity and reduction of electrode size at the level of single neuron. Among these, organic nanomaterials including conductive polymers (CPs) (Abidian et al., 2010; Green and Abidian, 2015), carbon nanotubes (CNTs) (Ansaldo et al., 2011) or graphene (Hess et al., 2011) have been popular choices that allow direct delivery of electrical, electrochemical and electromechanical signals at the electrode-tissue interface. Poly (3, 4-ethylenedioxythiophene) (PEDOT), which has excellent electronic conductivity (Fabretto et al., 2012; Maziz et al., 2015) providing low impedance and high capacitance (Abidian and Martin, 2009; Yoon and Jang, 2009) along with excellent biostability (Lecomte et al., 2017) and biocompatibility (Asplund et al., 2009) has been the most studied CP in

* Corresponding author. LAAS-CNRS, 7 avenue du Colonel Roche, F-31400, Toulouse, France.
** Corresponding author. LAAS-CNRS, Université de Toulouse, CNRS, F-31031 Toulouse, France.
E-mail addresses: christian.bergaud@laas.fr (C. Bergaud), ali.maziz@laas.fr (A. Maziz).

https://doi.org/10.1016/j.bios.2020.112413

the last decade (Fabretto et al., 2012). PEDOT-coated microelectrodes have been considered for biomedical (Smela, 2003) and bioelectronic applications (Berggren and Richter-Dahlfors, 2007), especially for the fabrication of devices for neuronal recording (Abidian et al. 2009, 2010; Castagnola et al., 2015; Lecomte et al., 2017) and stimulation (Cogan, 2008; Gerwig et al., 2012b; Venkatraman et al., 2009) as well as electrochemical sensing systems for neurochemicals monitoring (Larsen et al., 2012; Meng et al., 2019; Reddy et al., 2019; Su et al., 2017; Vreeland et al., 2015).

Through electrochemical deposition, PEDOT can be precisely localized onto metallic microelectrode sites with coating thicknesses down to the nanoscale. The oxidative deposition of PEDOT results in a positively charged polymer backbone, which allows for the incorporation of negatively charged doping agents for charge balancing. To date, the most commonly used dopant material for PEDOT material is poly (styrene sulfonate) (PSS) because of its stability and reported biocompatibility (Schmidt et al., 1997). However, other negatively charged dopants have been also utilized for this purpose, such as tosylate (Larsen et al., 2012), ClO_4^- (Maziz et al. 2014, 2017), Nafion (Vreeland et al., 2015) and more recently some carbonaceous nanomaterials such as carbon nanotubes CNTs (Gerwig et al., 2012b; Xu et al., 2013) or graphene oxide (GO) (Taylor et al., 2017) for the purpose of improving the electrochemical stability (Luo et al., 2011b), charge storage delivery (Gerwig et al., 2012b) and sensitivity of PEDOT electrodes for neurochemicals sensing (Wang et al., 2014; Weaver et al., 2014; Xu et al., 2013).

Carbon nanofibers (CNFs) are increasingly getting in the spotlight in bioanalytical area as through their properties of high surface area, non-toxicity and chemical and electrochemical stability. CNFs exhibit extraordinary strength and provide an extremely large surface area (compared to that of GO or PEDOT) for charge transfer and cell attachment, making them a very promising candidate material for recording and stimulation electrode sites (Nguyen-Vu et al., 2006). CNFs have also excellent electrical conductivity, which enables a better electron transfer at the interface of the electrode, and thus a better transduction of the electrochemical signal for redox-active molecules (Huang et al., 2008; Liu et al., 2008; Wu et al., 2007). Although direct substrate growth of the carbonaceous nanomaterials on metal-coated substrates has been used for the construction of biosensing devices (Koehne et al., 2011), very few studies have been performed regarding the micro-localized deposition of CNFs on any type of substrate (*e.g.* microelectrode array (MEA) or neural probes) due to the incompatibility of the CNF growing processes with most standard sensing devices (Koehne et al., 2011).

In this work, we report for the first time the electrochemical synthesis of PEDOT:CNF composite, and its deposition onto gold MEAs by a versatile and reproducible electrochemical route. PEDOT is electrochemically deposited to trap CNFs within its matrix, creating a nanocomposite in one step without the need of time-consuming grafting process (Fig. 1). We show that high-performance PEDOT:CNF composite exhibit remarkable electrochemical properties, yields microelectrodes combining low impedance, high surface area, high charge injection capability and can be effectively used for reliable neurotransmitters monitoring using amperometric techniques. Taken together, these results suggest the great potential of PEDOT:CNF composites for developing next-generation multifunctional bidirectional microelectrodes.

2. Materials and methods

The detailed experimental details are provided in Supplementary Information (SI).

3. Results and discussion

3.1. Electrochemical deposition

We initially fabricated PEDOT:CNF coatings and examined their morphology. As shown in Fig. 1B, we used microfabricated gold microelectrodes array, well-known tools allowing classical electrophysiological measurements. The microelectrodes have the same 20 µm diameter as commonly used for MEA arrays. We use this simple design to directly compare PEDOT:CNF to bare gold microelectrodes properties. First oxidized CNFs were synthesized for the following electrochemical synthesis of PEDOT:CNF composite (Fig. 1A). The oxidation of raw CNFs through oxidative acid treatment (mixture of H_2SO_4 and HNO_3) was crucial for the electrodeposition procedure. Previous reports showed that the oxidation of carbon nanomaterials not only enhanced their hydrophilicity but also created on their surfaces a range of oxygenated functions such as carboxylic groups through the oxidation reactions (Bortolamiol et al., 2014; Rasheed et al., 2007; Santangelo et al., 2012).

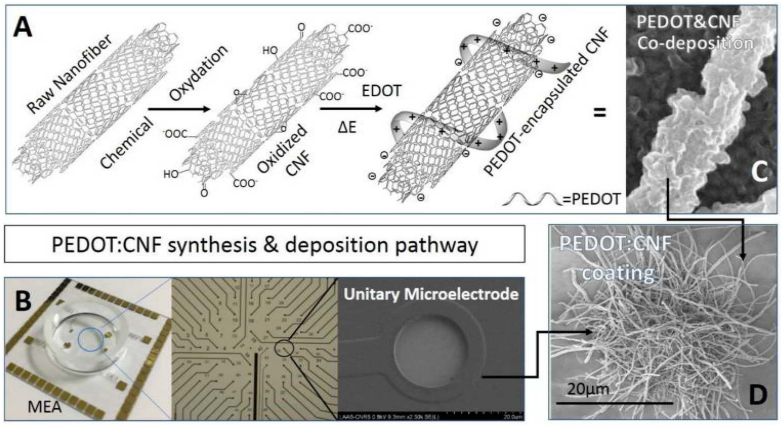

Fig. 1. PEDOT:CNF deposition pathway. (A) CNF functionalization scheme used for this study, from raw CNF to oxidized, negatively-charged CNFs obtained by chemical oxidation, which are used as dopants for co-deposition with positively-charged PEDOT. (B) Picture of the microfabricated gold microelectrodes array with optical picture of the microelectrode matrix and SEM picture of a single gold microelectrode (20 µm diameter). SEM pictures of the PEDOT:CNF composite obtained on (C) a macroelectrode and on (D) a microelectrode. (For interpretation of the references to colour in this figure legend, the reader is referred to the Web version of this article.)

The oxidized CNFs were consequently negatively charged due to the presence of carboxylate functional groups grafted at their surface, which made them a very interesting candidate for charge-balancing anionic PEDOT dopant. In this study, the PEDOT:CNF films were galvanostatically deposited onto gold microelectrodes at a constant current density of 10 pA/μm^2 until a total charge 1200 nC (3.821 nC/μm^2) was consumed (Fig. S1). The deposition took place through a simultaneous oxidative PEDOT polymer chain propagation and CNF trapping mechanisms, generating a fibrous and porous surface structure resulting from a three-dimensional growth mechanism of PEDOT around the oxidized CNFs (Fig. 1C and D) (Temmer et al., 2013). It is worth mentioning that an increase in the electrodeposition charge will result in a significant expansion of the PEDOT content in PEDOT:CNF composite while keeping it still rather localized. Nonetheless, the electrodeposition charge should not exceed 6 μC as it induces a subsequent expansion of the overall deposit, which weakens the overall mechanical stability of the film, leading to the delamination of the film, and/or causes short-circuits on the neighbor microelectrodes (Fig. S2).

3.2. Morphology

To confirm the structural integrity of the PEDOT:CNF coating and its interface with the underlying bare gold contact, a critical factor for the properties of the modified microelectrodes, we investigated the morphological stability of the PEDOT:CNF coating. Images with optical microscopy showed no obvious morphological cracking or visible delamination after the direct current deposition method (Fig. 2A). A quite uniform and highly dense CNFs coating could be observed on the modified microelectrode surface. To study further at the surface stability, the morphology of the PEDOT:CNF coating was observed by SEM. As shown in Fig. 2 (B and C), SEM images confirmed that the PEDOT:CNF composite was uniformly distributed on the gold microelectrode with CNF randomly distributed in the deposit. The PEDOT:CNF appeared as a porous fibrous 3D network encapsulated on the microelectrode. We have previously demonstrated that the electrochemically synthesized PEDOT:PSS film has a smoother surface with a globular structure resulting from a three-dimensional nucleation growth mechanism (Castagnola et al., 2014). The morphology of the PEDOT:CNF was thus very different from PEDOT:PSS. The CNFs integration in the PEDOT matrix is believed to be driven by electrostatic diffusion toward the electrode and encapsulation in the PEDOT matrix, resulting in a mechanically coherent composite. CNFs act as dopant thanks to the negative charges on the nanofibers surface, behaving like counter anion to EDOT radical-cation during electrochemical polymerization. In addition, the PEDOT density around the CNFs of the PEDOT:CNF network increased when increasing the electrochemical deposition charge (Fig. S3), confirming that the negatively charged CNFs act as dopants with positively charged PEDOT during the electropolymerization, with a strong templating effect on this polymerization. The evidence on the growth of the polymer and its interaction with the CNFs is further deduced from the Energy-dispersive X-ray spectroscopy (EDS) analysis (Fig. S4). EDS mapping was used to distinguish the sulfur content in PEDOT (and not present in the carbon nanofibers) and shows that the conducting PEDOT and carbon nanofibers are connected seamlessly, thereby facilitating intra- and interlayer ionic/electronic transport. The FT-IR spectra of the nanocomposite (Fig. S5) display the characteristic peaks of PEDOT at 920 and 985 cm^{-1}, which correspond to the C–S vibration modes of the thiophene ring in the PEDOT moiety. The absorption bands at 440, 850, 1070 and 1120 cm^{-1} represent the stretching modes of the C–O–C and O–C–C group of PEDOT in the nanocomposite whereas the peak at 1260 cm^{-1} indicates the C–C stretching mode of the thiophene (Anothumakkool et al., 2013; Shin et al., 2011; Tran-Van et al., 2001).

3.3. Electrochemical properties

High-performance electrodes materials play a crucial role at the interface of neural electrodes. To achieve efficient bidirectional transduction between the neural tissue and neural microelectrodes, the electrode material must satisfy the function of both ionic/electronic charge injection, to stimulate nerve tissue, and record neuronal activity. Ideally, the electrode material should offer seamless neural interfaces with desirable characteristics including low impedance to lower signal-to-noise ratio and so increase recorded potentials, and high charge storage capabilities which would be helpful for stimulation of neuron cells (Aqrawe et al., 2018).

We first evaluated the impact of the PEDOT:CNF deposition on the electrochemical properties of the microelectrodes by electrochemical impedance spectroscopy (EIS) and cyclic voltammetry (CV). Non-coated gold microelectrodes (identical diameter) were also tested as controls. Fig. 3A and B shows the Bode plots of the electrochemical impedance and phase angle across frequencies of interest for electrophysiological recordings (10 Hz–10 kHz). EIS analysis showed that the impedance of PEDOT:CNF microelectrode was more than two orders of magnitude lower than the bare microelectrode in the range of frequencies tested. The impedances of the microelectrodes at 1 kHz were used for comparison purposes as action potentials have a characteristic frequency band centered at that frequency. The mean impedance at 1 kHz for the unmodified gold microelectrode was around 600 kΩ, while after PEDOT:CNF electrochemical deposition, the mean impedance fell to 4.1 kΩ. This phenomenon is expected to be due to a significant increase in the effective surface area with the formation of PEDOT:CNF material, leading to the decrease in impedance of the microelectrode (Castagnola et al., 2014). Furthermore, the specific impedance of the PEDOT:CNF

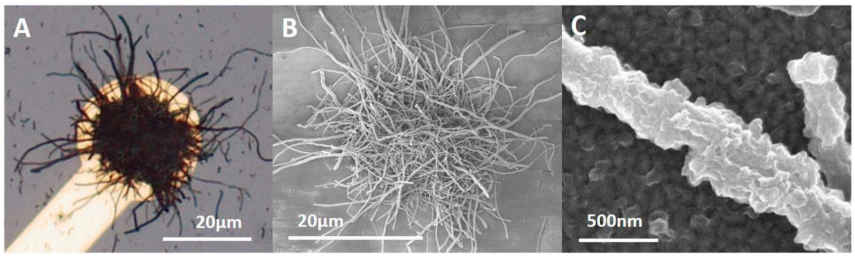

Fig. 2. Morphological characterization of PEDOT-CNF microelectrodes. Microscope picture of (A) PEDOT-CNF modified gold microelectrode (20 μm diameter). (B) SEM picture of PEDOT-CNF modified microelectrode. (C) SEM picture of a CNF encapsulated in PEDOT, with a PEDOT layer underneath it, deposit done with a current density of 10 pA/μm^2 on a 1 cm^2 gold macroelectrode. (For interpretation of the references to colour in this figure legend, the reader is referred to the Web version of this article.)

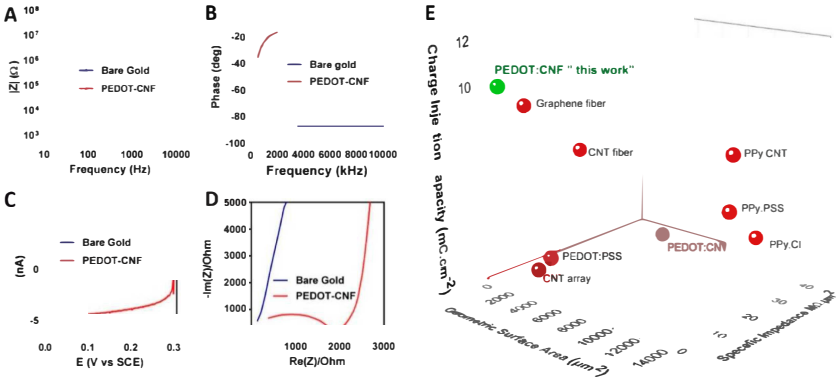

Fig. 3. Electrochemical characterization of PEDOT:CNF modified microelectrodes. (A) EIS measurements on modified PEDOT:CNF and unmodified gold microelectrodes over a frequency range of 10 Hz-10 kHz in H_2SO_4 (0.5 M) at 0 V *vs* SCE A) |Z| *vs* frequency and (B) Phase *vs* frequency plots. (C) Capacitive measurements by cyclic voltammetry in H_2SO_4 (0.5 M) at 50 mV/s between 0 and 0.3 V *vs* SCE on modified and unmodified (Fig. S7) microelectrodes. (D) Nyquist plots of modified PEDOT:CNF and unmodified gold microelectrodes over a frequency range of 10 Hz-7 MHz in H_2SO_4 (0.5 M) at 0 V *vs* SCE. (E) Comparison of the electrochemical performances of PEDOT:CNF microelectrodes in terms of charge injection limit, specific impedance at 1 kHz, and geometrical area of the starting modified microelectrodes with some of the state-of-art nanostructured organic materials used for neural interfacing electrodes. The corresponding values and references are reported in Table S1. (For interpretation of the references to colour in this figure legend, the reader is referred to the Web version of this article.)

modified microelectrodes (1.28 MΩ μm^2 at 1 kHz) was *ca.* 150 times lower than gold microelectrodes (188 MΩ μm^2) and lower than any of the best reported organic electrode materials (Wang et al., 2019) including conducting polymers *e.g.* PEDOT:PSS (Venkatraman et al., 2011) and PPy:PSS (Wang et al., 2019), CNTs (Wang et al., 2006) and neat graphene (Wang et al., 2019) nanomaterials, presented in Fig. 3D and Table S1. The combination of CNFs and PEDOT as a single composite material thus resulted in a strong synergetic effect leading to a superior microelectrode with lower impedance.

The phase plot of the impedance showed that PEDOT:CNF was capacitive in the low frequency range (10 Hz) (Fig. 3B), with a phase angle around 80–90°. The phase angle decreased for the coated microelectrodes in the frequency range of 10 Hz-2 kHz to ≈20°, while the phase angle of bare gold was about 90°. The shift in the phase of the impedance for modified PEDOT:CNF suggests an increase in effective surface area. Such changes were consistent with previous findings where carbon nanotubes were incorporated in the PEDOT matrix as a single composite material (Kozai et al., 2016; Xu et al., 2013; Zhou et al., 2013). These results show that PEDOT:CNF acts as a capacitive material for frequencies lower than 2 kHz and as a more-resistive material for frequencies higher than 2 kHz. The Nyquist plot recorded in H_2SO_4 media is presented in Fig. 3D. In the higher frequency region, a semi-circle is observed which is related to the charge resistance between the electrode material and the surrounding electrolyte while at low frequencies the capacitive behavior becomes dominant. The incorporation of CNF in the PEDOT produced very small radius of the semi-circle on the Nyquist plot with a charge transfer resistance of about 1.9 kΩ as estimated from an equivalent circuit (Fig. S6). This result proves the low electron-transfer resistance associated with the PEDOT:CNF composite material, by which the electronic exchange in the systems is expected to be favored.

We next evaluated the charge transfer capabilities of the PEDOT:CNF microelectrodes. CVs have been carried out within the 0.0 to +0.3 V potential range at a scan rate of 50 mV/s. Compared to the bare gold microelectrode (Fig. 3C and Fig. S7), a significant increase in the electroactive area could be clearly observed. The capacity of charge transfer observably increased using PEDOT:CNF, as can be seen in Fig. 3C. The cathodal CSC (CSCc) of the composite film was calculated by the time integral of the cathodal currents within the cycled region. Obviously, the CSCc of the PEDOT:CNF coated microelectrode is significantly higher than that of bare gold microelectrode (≈80 times). At a density of 10 pA/μm^2 that was applied to electrodeposit the materials, the CSCc of the bare gold microelectrode increased from 0.1 mC/cm^2 to 7.89 mC/cm^2 for PEDOT:CNF within the 0.0–0.3 V potential range. This improvement is due to the higher surface area coating the PEDOT:CNF that allows effective diffusion of electrolyte ions at the electrode-solution interface, leading to a higher charge storage capability. It is worth mentioning that the symmetry of the cyclic voltammograms of the PEDOT:CNF coating is an indication of the high reversibility of the doping process, which makes the composite material a promising material as ionic-to-electronic transducer at the neural interface electrode.

3.4. *Electrical stimulation*

The previously calculated charge capacity value can only be regarded as relative value, as it measures the charge capacity of the electrodes when subjected to a slow voltage ramp. In neural stimulation applications, cathodal-first, biphasic current pulses are frequently used for effective and safe stimulation of neural tissue (Gerwig et al., 2012a; Luo et al., 2011a; Mandal et al., 2015). The electrodes conduct a high number of electrical stimuli when using only millisecond current pulses, therefore only a small fraction of the total charge capacity is available. Here, we used voltage transient responses to millisecond biphasic current pulses to have a more reliable information about the microelectrode stimulation performance.

Fig. 4 reports the voltage transients measurements that were collected by the PEDOT:CNF and bare gold microelectrodes, using 1 ms-long biphasic current pulses with cathodic pulse first in a physiological media-mimicking buffer, Tris buffer 1X at pH = 7.4. For a given pulse current, the preferred electrode should have a higher charge injection capability and generate lower electrode voltage, thanks to its higher charge transfer capability. Starting with a series of small pulses of ±1.256 μA corresponding to 4 pC/μm^2 (Fig. 4A), the highest cathodic voltage transient was observed for non-coated gold microelectrode, producing maximum negative voltage $V_{max,neg}$ of −1.92 V (Fig. 4B–D). Under the same stimulation conditions, the amplitude of voltage

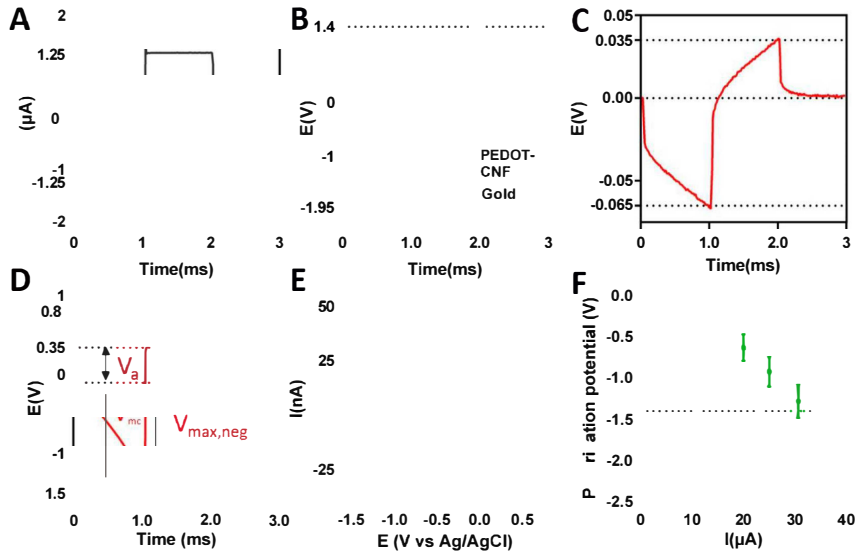

Fig. 4. *In vitro* biphasic stimulation assessment. (A) Biphasic excitation current waveform (±1.256 μA, 1 ms) tested *in vitro* in Tris buffer 1X, cathodic pulse first. (B) Voltage responses of PEDOT-CNF modified microelectrodes and bare gold microelectrode. (C) Voltage transient of PEDOT:CNF microelectrodes only. (D) Voltage transient of a PEDOT:CNF-modified microelectrode at 31.5 μA injection, when reaching the CIL. (E) Cyclic voltammetry of PEDOT:CNF modified microelectrodes in Tris buffer 1X, at 200 mV/s. (F) Polarization potentials measured under different current pulse amplitudes. (For interpretation of the references to colour in this figure legend, the reader is referred to the Web version of this article.)

transient is much less in PEDOT:CNF coated microelectrode producing $V_{max,neg}$ of −0.067 V. These values correspond to V_{mc} (maximum negative polarization voltage) across electrode-electrolyte interface of −37 mV for PEDOT:CNF (Fig. 4 C and D). The negative potential excursion V_{mc} was calculated by subtracting the access voltage (V_a), associated with the ohmic resistance of the electrolyte from the maximum negative voltage $V_{max,neg}$ (Carli et al., 2018). Indeed, voltage excursion displays first an initial ohmic voltage drop followed by a more gradual polarization of the interface as shown in Fig. 4D. Due to increased charge carriers at the interface, less polarization is seen at the PEDOT:CNF interface compared to gold microelectrodes. In this condition, the voltage drop V_a was observed for PEDOT:CNF in the order of 29 mV, and 30 times higher for gold microelectrodes with 0.9 V, suggesting a substantially lower overpotential to be overcome in PEDOT:CNF microelectrodes. This result is in agreement with the electrochemical CV characterization that gives a higher electroactive surface area (Fig. 3C) for PEDOT:CNF with respect to bare gold control. The voltage transient experiments reflect the obvious improvement by PEDOT:CNF coating in delivering in a safer manner, for a stimulation current, a higher charge at the electrode-electrolyte interface.

To fully assess the applicability of the PEDOT:CNF microelectrodes for tissue stimulation purposes, their charge injection limit (CIL) was measured using increasing pulse currents (Fig. 4F). The CIL is defined as the quantity of charge that can move from the electrode to the solution in a stimulation pulse without exceeding the water electrolysis limits. To ensure the safe polarization, the water window of the PEDOT:CNF microelectrodes in Tris buffer solution was determined using CV at 200 mV/s *vs* Ag/AgCl reference electrode (Fig. 4E). The water reduction and oxidation voltages were found to be at −1.4 and 0.6 V respectively. The polarization voltage V_{mc} was used to determine the CIL by increasing the pulse currents before V_{mc} is reaching the negative electrolysis frontier at −1.4 V. The measured corresponding maximum current before the water reduction potential was 31.5 ± 3.4 μA (Fig. 4F). The calculated charge injection was calculated at $V_{mc=}$−1.3 V, before the water reduction potential to be 10.032 ± 1.083 mC/cm^2 for the PEDOT:CNF microelectrodes. The calculated CIL of the composite material was higher than any of the best reported organic materials (Wang et al., 2019) including PEDOT:PSS (2.92 mC/cm^2) (Venkatraman et al., 2011), CNTs array (1–1.6 mC/cm^2) (Wang et al., 2006), PEDOT:CNT (1.25 mC/cm^2) (Gerwig et al., 2012b) or neat graphene fibers (8.9 mC/cm^2) (Wang et al., 2019) presented in Fig. 3D and Table S1. These voltage transient experiments reflect the obvious improvement by PEDOT:CNF coating of delivering in a safer manner, for a stimulation current, a higher charge at the microelectrode-electrolyte interface. We believe that the combination of CNFs with high charge transfer capabilities and PEDOT results in as strong synergetic effect between the two components in the composite leading to remarkable charge injection capacity.

3.5. *Electrochemical sensing*

To demonstrate the extended functional aspects of the PEDOT:CNF composite, we explored the electrochemical sensing capabilities of the modified microelectrodes in a non-specific fashion of biomolecules, specifically neurotransmitters such as dopamine (DA) and serotonin (ST). DA and ST are ubiquitous neurotransmitters in mammalian brain tissues, and together with other neurotransmitters, play an important physiological role in the functioning of central nervous as extra cellular chemical messengers (Beaulieu and Gainetdinov 2011; Carhart-Harris and Nutt, 2017). These biological analytes are commonly found together and their biodetection using macro-scaled unitary carbon fiber microelectrode has been the focus of a tremendous number of reports in the last decades (Vreeland et al., 2015; Wang et al., 2014; Weaver et al., 2014). However, it remains challenging to use similar electrode material deposited on localized electrodes on any type of substrate *e.g.* MEAs,

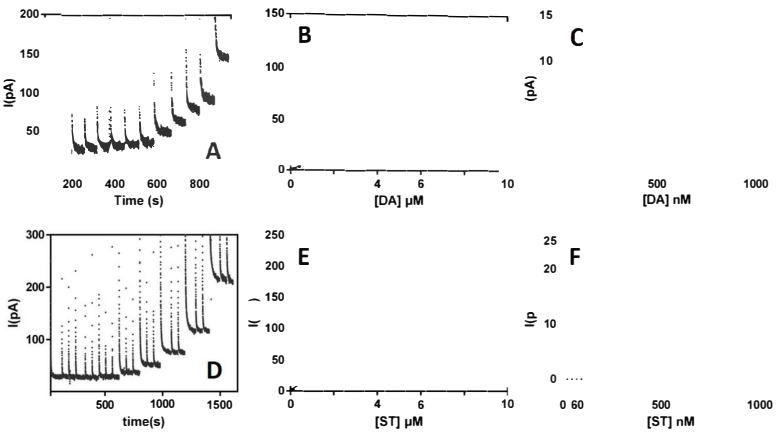

Fig. 5. *In vitro* electrochemical sensing. Typical chronoamperometric response of a PEDOT-CNF microelectrode to (A) dopamine and (D) serotonin injections in Tris 1X. At +130 mV *vs* SCE for dopamine detection and 328 mV *vs* SCE for serotonin detection. The currents steps in the figure correspond to (A) 100, 200, 300, 400, 600, 800 nM and 1, 2, 3, 4, 5, 9 µM and (B) 60, 100, 400 nM and 1, 2, 4, 9 µM. Linear regression curve of PEDOT-CNF electrode response at 130 mV *vs* SCE to (B) DA and (E) ST in Tris buffer. Zoom in on the region between 0 and 1 µM for (C) DA and (F) ST.

neural probes or drug delivery devices, as very few reports have been produced using non-unitary carbon-based microelectrodes materials (Koehne et al., 2011).

Initially, CV experiments in Tris buffer solution (pH = 7.4) with varying concentrations of DA and ST were used to identify the oxidation potentials of both DA and ST (Figs. S8 and S9). PEDOT:CNF coated microelectrodes were used as working electrode, while SCE and platinum were respectively used as reference and counter electrodes. According to the CV results, 130 mV and 328 mV *vs* SCE were chosen for the following chronoamperometric detection of DA and ST, respectively. In separate experiments, specific amounts of DA and ST were added to Tris buffer (pH = 7.4) at various intervals after stabilization of background current. A sharp anodic increase in the current was obtained for each addition of analyte, which was attributed to the fast, direct electrochemical oxidation of the analyte at the electrode vicinity. A typical chronoamperometric responses obtained with a PEDOT-CNF modified microelectrode is shown in Fig. 5 (A and D). The response of the PEDOT:CNF at the modified microelectrode was reached within 15 s, revealing the fast diffusion of the PEDOT:CNF on the microelectrode site. The current response increased linearly in the concentration range from 0.1 to 9 µM for DA and from 0.06 to 9 µM for ST (Fig. 5 B, C, E and F). The DA and ST direct current responses resulted in calibration plots *i.e.* amperometric current response *vs.* different concentration of DA or ST with correlation coefficients >0.999 for both DA and ST. The corresponding sensitivities were calculated as 14.3 pA/µM with the limit of detection (LOD) of 0.045 µM for dopamine and 22.32 pA/µM with a LOD of 0.056 µM for serotonin. In terms of concentration ranges, these LOD were well suited to the reported assay of these analytes in the medical field (Polidori et al., 2001). The stability of the proposed electrochemical biosensor was evaluated (Fig. S10). A 10% drop in sensitivity was observed after 5 h of continuous exposure of a polarized electrode to 1 µM of DA in Tris buffer. Sensitivity can be restored by acidic rinsing of the microelectrode with H_2SO_4 0.5 M. This sensitivity drop is believed to be due to dopamine adsorption, which correlate with the fact that it is reversible by electrode rinsing. The analytical performance of the fabricated PEDOT:CNF microelectrode (LOD, sensitivity and linear response range) of the sensor was compared with previously reported DA sensors using chronoamperometric technique (Table S2). It can be seen that the PEDOT:CNF is comparable or better with the previously reported DA sensors, hence it can be used for sensitive detection of neurotransmitters in biological analysis. The good analytical performance of the PEDOT:CNF towards neurochemical detection was attributed to the huge reactive surface area and excellent electron transfer rate, which has been shown to catalyze electron transfer at the electrode-electrolyte interface.

3.6. *In vitro cytotoxicity assay*

In addition to excellent electrical and electrochemical properties, the PEDOT:CNF composite material should being free of toxic elements, to be used as an *in vivo* neural interface. PEDOT-based materials on gold microelectrodes are commonly used for neural cell culturing and have been proven to be a biocompatible material with living systems useable to design neural interfaces (Asplund et al., 2009). Through cell viability assay, we set the preliminary objective to establish the non-cytotoxicity of the produced composite, after the electrochemical deposition. For that purpose, cytotoxicity was investigated with the MTT cell viability assay (ISO 10993–5 norm). Two populations of cells were cultured for 24 h and then one population was exposed for 24 h to culture media containing PEDOT:CNF material extracts. After 48 h, MTT test was performed on both populations, in the test media and in a standard media as control. The results show that the population of living SH-SY5Y cells increases over time in a similar fashion for controls, demonstrating that no cytotoxicity could be observed as viability percentage highly exceeds 75% (>99%).

3.7. *Cells growth & morphology studies*

To study to possibility of cells to grow on modified surfaces, human neuroblastoma SH-SY5Y cells were cultivated on PEDOT:CNF-modified MEAs to investigate the cell adhesion and neurite outgrowths on the modified microelectrodes. As shown in Fig. 6 (A and C), After 24 and 72 h, SH-SY5Y cells grew uniformly and appeared to have spread homogeneously, demonstrating a good viability on the MEA substrate, even at 24 h, as no cell repulsion was found around coated electrodes. In order to investigate the state of SH-SY5Y cells cultured in detail, further work was conducted by fluorescent staining. As shown in Fig. 6 (B and D), SH-SY5Y cells grew evenly overall, and neurites were clearly observed on the composite materials. These results indicate that PEDOT:CNF composite is well-suited for the adhesion and neurite outgrowth of SH-SY5Y cells.

The morphology of the cells on the PEDOT:CNF microelectrodes was also assessed through SEM. SH-SY5Y cells were seeded in the MEA and cultured for 48 h, then the fixation procedure was performed before proceeding to the SEM observation. Individual cells can be clearly recognized on the top of the PEDOT:CNF microelectrodes in Fig. 6 (E and

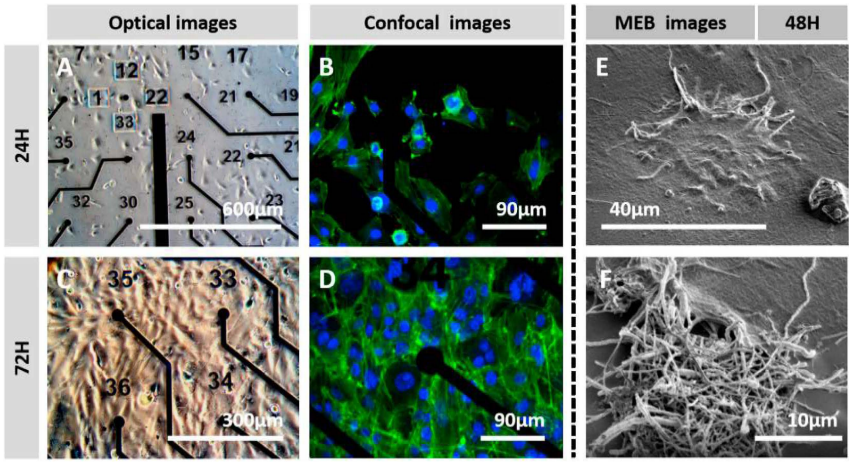

Fig. 6. *In vitro* cytotoxicity assay & cell morphology assessment. Optical images showing SH-SY5Y cultivated on top of the PEDOT:CNF coated microelectrodes array for (A) 24 h and (C) 72 h. The corresponding phalloidin-AM fluorescent images showing SH-SY5Y cultivated on top of the PEDOT:CNF coated microelectrodes array for (B) 24 h and (D) 72 h. SEM images of SH-SY5Y cells cultured 48 h on functionalized PEDOT:CNF microelectrodes surface. (E) Cell completely interfaced in 3D-manner with a PEDOT:CNF-modified microelectrode, with clear interfacing with fiber network of the electrode. (F) PEDOT:CNF microelectrode being colonized a cell.

F). The SH-SY5Y cells display extensive processes and appear to be well attached on the surface of the PEDOT:CNF material. It is worth mentioning that the cells did not exhibit any particular preference for different materials *i.e.* gold or MEA passivation layer and, as can be observed, they spread homogeneously on the surface of the MEA. The attachment of cells on PEDOT:CNF coated microelectrode shown in SEM images means that it is possible to the get direct, reliable and functional contact with the target tissue required for interfacing purposes. For example, when accurate electrophysiology recordings are required, a single unit may be detected and recorded when the recording device is very close from the targeted single neuron.

4. Conclusions

We have successfully demonstrated the feasibility of PEDOT:CNF composite material on gold microelectrode arrays by a simple and reproducible electrodeposition method. PEDOT was used to electrochemically entrap oxidized carbon nanofibers as dopants in one step, without the need of time-consuming multi-step processes. The combination of CNFs and PEDOT resulted in as strong synergetic effect between the two components in the composite leading to remarkable electrochemical properties, combining low impedance, high charge injection capability, as well as a reliable neurotransmitter monitoring. The results from this study suggest the great potential of PEDOT:CNF composites for developing next-generation microelectrodes for applications in neural therapies. We are currently running *in vivo* studies to show that PEDOT:CNF microelectrodes implanted in the cerebral cortex can detect neuronal activity with remarkably high signal-to-noise ratio in an area as small as an individual neuron. We also envision the use the PEDOT:CNF microelectrodes for neurochemicals monitoring *in vitro* and *in vivo* using fast scan cyclic voltammetry techniques.

Funding sources

This work was supported by ANR Neuro MEDDLE Grant ANR-15-CE19-0006 and ANR 3DBrain Grant ANR-19-CE19-0002-01.

Declaration of competing interest

The authors declare that they have no known competing financial interests or personal relationships that could have appeared to influence the work reported in this paper.

CRediT authorship contribution statement

Valentin Saunier: Investigation, Writing review & editing. **Emmanuel Flahaut:** Investigation, Writing - review & editing. **Marie-Charline Blatché:** Investigation, Validation. **Christian Bergaud:** Supervision, Resources, Investigation, Writing - review & editing. **Ali Maziz:** Supervision, Resources, Methodology, Investigation, Writing - review & editing.

Acknowledgment

We thank Dr. Anne-Marie Galibert and Dr. Brigitte Soula (CIRIMAT, Université de Toulouse, CNRS, F-31062, France) for help in the work on raw carbon nanofibers. We thank M. Jean-Baptiste Doucet and M. Julien Roul for help and guidance during FT-IR measurements. The authors acknowledge fundings from the Agence Nationale de la Recherche (ANR-15-CE19-0006 and ANR-19-CE19-0002-01). This work was supported by French RENATECH network.

Appendix A. Supplementary data

Supplementary data to this article can be found online at https://doi.org/10.1016/j.bios.2020.112413.

References

Abidian, M.R., Martin, D.C., 2009. Adv. Funct. Mater. 19 (4), 573–585.
Abidian, M.R., Corey, J.M., Kipke, D.R., Martin, D.C., 2010. Small 6 (3), 421–429.
Abidian, M.R., Ludwig, K.A., Marzullo, T.C., Martin, D.C., Kipke, D.R., 2009. Adv. Mater. 21 (37), 3764 3770.
Andrews, R.J., 2009. Progress in Brain Research. Elsevier, pp. 127–139.

Anothumakkool, B., Bhange, S.N., Unni, S.M., Kurungot, S., 2013. RSC Adv. 3 (29), 11877–11887.
Ansaldo, A., Castagnola, E., Maggiolini, E., Fadiga, L., Ricci, D., 2011. ACS Nano 5 (3), 2206–2214.
Aqrawe, Z., Montgomery, J., Travas-Sejdic, J., Svirskis, D., 2018. Sensor. Actuator. B Chem. 257, 753 765.
Asplund, M., Thaning, E., Lundberg, J., Sandberg-Nordqvist, A.C., Kostyszyn, B., Inganäs, O., Von Holst, H., 2009. Biomed. Mater. 4 (4).
Beaulieu, J.M., Gainetdinov, R.R., 2011. Pharmacol. Rev. 63 (1), 182–217.
Berggren, M., Richter-Dahlfors, A., 2007. Adv. Mater. 19 (20), 3201 3213.
Bortolamiol, T., Lukanov, P., Galibert, A.-M., Soula, B., Lonchambon, P., Datas, L., Flahaut, E., 2014. Carbon 78, 79–90.
Carhart-Harris, R.L., Nutt, D.J., 2017. J. Psychopharmacol. 31 (9), 1091–1120.
Carli, S., Lambertini, L., Zucchini, E., Ciarpella, F., Scarpellini, A., Prato, M., Castagnola, E., Fadiga, L., Ricci, D., 2018. Sensor. Actuator. B Chem. 271, 280–288.
Castagnola, V., Bayon, C., Descamps, E., Bergaud, C., 2014. Synth. Met. 189, 7–16.
Castagnola, V., Descamps, E., Lecestre, A., Dahan, L., Remaud, J., Nowak, L., Bergaud, C., 2015. Biosens. Bioelectron. 67, 450–457.
Cogan, S.F., 2008. Annu. Rev. Biomed. Eng. 10, 275–309.
Fabretto, M.V., Evans, D.R., Mueller, M., Zuber, K., Hojati-Talemi, P., Short, R.D., Wallace, G.G., Murphy, P.J., 2012. Chem. Mater. 24 (20), 3998–4003.
Gerwig, R., Fuchsberger, K., Schroeppel, B., Link, G.S., Heusel, G., Kraushaar, U., Schuhmann, W., Stett, A., Stelzle, M., 2012a. Front. Neuroeng. 5, 8.
Gerwig, R., Fuchsberger, K., Schroeppel, B., Link, G.S., Heusel, G., Kraushaar, U., Schuhmann, W., Stett, A., Stelzle, M., 2012b. Front. Neuroeng. 5, 8.
Green, R., Abidian, M.R., 2015. Adv. Mater. 27 (46), 7620–7637.
Heim, M., Yvert, B., Kuhn, A., 2012. J. Physiol. Paris 106 (3-4), 137–145.
Hess, L.H., Jansen, M., Maybeck, V., Hauf, M.V., Seifert, M., Stutzmann, M., Sharp, I.D., Offenhäusser, A., Garrido, J.A., 2011. Adv. Mater. 23 (43), 5045–5049.
Huang, J., Liu, Y., Hou, H., You, T., 2008. Biosens. Bioelectron. 24 (4), 632–637.
Koehne, J.E., Marsh, M., Boakye, A., Douglas, B., Kim, I.Y., Chang, S.-Y., Jang, D.-P., Bennet, K.E., Kimble, C., Andrews, R., 2011. Analyst 136 (9), 1802–1805.
Kozai, T.D., Catt, K., Du, Z., Na, K., Srivannavit, O., Haque, R.U., Seymour, J., Wise, K.D., Yoon, E., Cui, X.T., 2016. IEEE Trans. Biomed. Eng. 63 (1), 111–119.
Larsen, S.T., Vreeland, R.F., Heien, M.L., Taboryski, R., 2012. Analyst 137 (8), 1831–1836.
Lecomte, A., Degache, A., Descamps, E., Dahan, L., Bergaud, C., 2017. Sensor. Actuator. B Chem. 251, 1001–1008.
Liu, Y., Huang, J., Hou, H., You, T., 2008. Electrochem. Commun. 10 (10), 1431–1434.
Ludwig, K.A., Uram, J.D., Yang, J., Martin, D.C., Kipke, D.R., 2006. J. Neural. Eng. 3 (1), 59.
Luo, X., Weaver, C.L., Zhou, D.D., Greenberg, R., Cui, X.T., 2011a. Biomaterials 32 (24), 5551–5557.
Luo, X., Weaver, C.L., Zhou, D.D., Greenberg, R., Cui, X.T., 2011b. Biomaterials 32 (24), 5551–5557.
Mandal, H.S., Kastee, J.S., McHail, D.G., Rubinson, J.F., Pancrazio, J.J., Dumas, T.C., 2015. Neuromodulation 18 (8), 657–663.
Maziz, A., Simaite, A., Bergaud, C., 2017. Polymerized Ionic Liquids. Royal Society of Chemistry, pp. 456–488.
Maziz, A., Plesse, C., Soyer, C., Cattan, E., Vidal, F., 2015. ACS Applied Materials & Interfaces.
Maziz, A., Plesse, C., Soyer, C., Chevrot, C., Teyssié, D., Cattan, E., Vidal, F., 2014. Adv. Funct. Mater. 24 (30), 4851–4859.
Meng, L., Turner, A.P., Mak, W.C., 2019. ACS Appl. Mater. Interfaces 11 (37), 34497 34506.
Nguyen-Vu, T.B., Chen, H., Cassell, A.M., Andrews, R., Meyyappan, M., Li, J., 2006. Small 2 (1), 89–94.
Nicolelis, M.A., Dimitrov, D., Carmena, J.M., Crist, R., Lehew, G., Kralik, J.D., Wise, S.P., 2003. Proc. Natl. Acad. Sci. Unit. States Am. 100 (19), 11041–11046.
Polidori, M.C., Stahl, W., Eichler, O., Niestroj, I., Sies, H., 2001. Free Radic. Biol. Med. 30 (5), 456–462.
Polikov, V.S., Tresco, P.A., Reichert, W.M., 2005. J. Neurosci. Methods 148 (1), 1–18.
Rasheed, A., Howe, J.Y., Dadmun, M.D., Britt, P.F., 2007. Carbon 45 (5), 1072–1080.
Rebscher, S.J., Hetherington, A., Bonham, B., Wardrop, P., Whinney, D., Leake, P.A., 2008. J. Rehabil. Res. Dev. 45 (5), 731.
Reddy, S., Xiao, Q., Liu, H., Li, C., Chen, S., Wang, C., Chiu, K., Chen, N., Tu, Y., Ramakrishna, S., 2019. ACS Appl. Mater. Interfaces 11 (20), 18254–18267.
Santangelo, S., Messina, G., Faggio, G., Abdul Rahim, S.H., Milone, C., 2012. J. Raman Spectrosc. 43 (10), 1432–1442.
Schmidt, C.E., Shastri, V.R., Vacanti, J.P., Langer, R., 1997. Proc. Natl. Acad. Sci. Unit. States Am. 94 (17), 8948–8953.
Shin, H.-J., Jeon, S.S., Im, S.S., 2011. Synth. Met. 161 (13-14), 1284–1288.
Smela, E., 2003. Adv. Mater. 15 (6), 481–494.
Su, C.-H., Sun, C.-L., Liao, Y.-C., 2017. ACS Omega 2 (8), 4245–4252.
Taylor, I.M., Robbins, E.M., Catt, K.A., Cody, P.A., Happe, C.L., Cui, X.T., 2017. Biosens. Bioelectron. 89, 400–410.
Temmer, R., Maziz, A., Plesse, C., Aabloo, A., Vidal, F., Tamm, T., 2013. Smart Mater. Struct. 22 (10), 104006.
Tran-Van, F., Garreau, S., Louarn, G., Froyer, G., Chevrot, C., 2001. J. Mater. Chem. 11 (5), 1378–1382.
Venkatraman, S., Hendricks, J., Richardson-Burns, S., Jan, E., Martin, D., Carmena, J.M., 2009. 4th International IEEE/EMBS Conference on Neural Engineering. IEEE, pp. 383–386.
Venkatraman, S., Hendricks, J., King, Z., Sereno, A., Richardson-Burns, S., Martin, D., Carmena, J., 2011. IEEE Transactions on 19, 307–316.
Vreeland, R.F., Atcherley, C.W., Russell, W.S., Xie, J.Y., Lu, D., Laude, N.D., Porreca, F., Heien, M.L., 2015. Anal. Chem. 87 (5), 2600–2607.
Wagenaar, D.A., Madhavan, R., Pine, J., Potter, S.M., 2005. J. Neurosci. 25 (3), 680–688.
Wang, K., Fishman, H.A., Dai, H., Harris, J.S., 2006. Nano Lett. 6 (9), 2043 2048.
Wang, K., Frewin, C.L., Esrafilzadeh, D., Yu, C., Wang, C., Pancrazio, J.J., Romero-Ortega, M., Jalili, R., Wallace, G., 2019. Adv. Mater. 31 (15), 1805867.
Wang, W., Xu, G., Cui, X.T., Sheng, G., Luo, X., 2014. Biosens. Bioelectron. 58, 153–156.
Weaver, C., Li, H., Luo, X., Cui, X., 2014. J. Mater. Chem. B 2 (32), 5209 5219.
Wu, L., Zhang, X., Ju, H., 2007. Anal. Chem. 79 (2), 453–458.
Xu, G., Li, B., Cui, X.T., Ling, L., Luo, X., 2013. Sensor. Actuator. B Chem. 188, 405–410.
Yoon, H., Jang, J., 2009. Adv. Funct. Mater. 19 (10), 1567–1576.
Zhou, H., Cheng, X., Rao, L., Li, T., Duan, Y.Y., 2013. Acta Biomater. 9 (5), 6439–6449.